Current Applied Physics 13 (2013) 710–716

Contents lists available at SciVerse ScienceDirect

Current Applied Physics

journal homepage: www.elsevier.com/locate/cap

Structural and optical properties of pulsed laser deposited ZnO thin films

E. Fazio [a], S. Patanè [a], S. Scibilia [a], A.M. Mezzasalma [a], G. Mondio [a], F. Neri [a], S. Trusso [b,*]

[a] Dipartimento di Fisica e di Scienze della Terra, Università di Messina, Viale Ferdinando Stagno d'Alcontres 31, I-98166 Messina, Italy
[b] CNR-Istituto per i Processi Chimico Fisici, Viale Ferdinando Stagno d'Alcontres 37, 98158 Messina, Italy

ARTICLE INFO

Article history:
Received 1 August 2012
Received in revised form
17 November 2012
Accepted 22 November 2012
Available online 30 November 2012

Keywords:
Zinc oxide
Nanostructures
Pulsed laser ablation
Optical properties
Raman scattering
AFM

ABSTRACT

Nanocrystalline ZnO thin films were grown by means of pulsed laser deposition. The ablation process was carried out at relatively low background oxygen gas pressure (10 Pa) and by varying the substrate temperature up to 600 °C. Information on the structural and morphological properties of the deposited thin films have been obtained by means of X-ray photoelectron, Raman spectroscopies, X-ray diffraction (XRD) and atomic force microscopy (AFM). The results showed that all the deposited films are sub-stoichiometric in oxygen and with a hexagonal wurtzite crystalline structure, characterized by features of some tens of nanometers in size. An improvement of the films' crystalline quality was observed for the deposition temperature of 300 °C while the further increase of the deposition temperature up to 600 °C induces a worsening of the material's structural properties with the development of a large amount of nanoparticle's clusters. The analysis of the XRD patterns shows a growth crystallographic preferential direction as a function of the deposition temperature, in agreement with the appearance of the only E_2 optical phonon mode in the Raman spectra. Such findings are compatible with the changes observed in the photoluminescent (PL) optical response and was related to the modification of the ZnO thin film structural quality.

1. Introduction

Zinc oxide (ZnO) is a II–VI binary semiconductor with a direct band gap in the near-UV spectral region (3.3 eV at room temperature), good optical transmittance (90%) in the visible region, large free-exciton binding energy (60 meV) so that excitonic emission processes can persist even above the room temperature. Thanks to these properties, ZnO has been widely used as UV or blue-emitting material in a broad range of applications, including transparent electrodes for flat-panel displays, p–n junction diodes, thin film transistors and solar cells [1–3].

ZnO crystallizes in the wurtzite structure, as gallium nitride (GaN), but its availability in large bulk single crystals is a big advantage over GaN [4]. Otherwise, the use of ZnO as a semiconductor in electronic devices is hindered by the lack of control over its electrical conductivity, due to a typical n-type semiconducting behavior [5]. Furthermore, ZnO has been recently considered as a substrate for GaN, to which it provides a close match [6]. This revival of interest toward ZnO as an optoelectronic or electronic material in its own right has required a significant improvement in the quality of ZnO single crystal substrates and thin films, trying to achieve a p-type conductivity [4,7]. Theoretical studies have also contributed to a deeper understanding of the role of native point defects and impurities on the unintentional ZnO n-type conductivity [8,9].

It was found that the properties of the ZnO thin films are affected by many factors such as morphology, composition and distribution of the ZnO nanostructures which, in turn, depend on the deposition process adopted [10–12]. ZnO thin films can be deposited by means of different techniques such as metal-organic chemical vapor deposition [13], electrochemical processing [14], spray pyrolysis [15], molecular beam epitaxy [16], radio frequency magnetron sputtering [17] and pulsed laser deposition (PLD) [18]. Among them, PLD presents at least two relevant characteristics suitable to obtain device-grade quality thin films at relatively low temperature: an intrinsically high energetic content of species that can be controlled by the laser pulse energy, the possibility to grow hydrogen-free films from a solid precursor and a great flexibility in the control of several deposition parameters (laser fluence and wavelength, target composition, substrate temperature, target–substrate distance and the possibility of performing the process in a controlled, either inert or reactive, background atmosphere) [19–21]. The possibility of a relatively easy control of the PLD processing parameters has allowed the preservation of the

* Corresponding author. Tel.: +39 (0)90 39762210; fax: +39 (0)90 3974130.
E-mail address: trusso@me.cnr.it (S. Trusso).

1567-1739/$ – see front matter © 2012 Elsevier B.V. All rights reserved.
http://dx.doi.org/10.1016/j.cap.2012.11.010

stoichiometry in going from the target to the thin film with relatively uniform and high dense nanostructures [22]. These systems show unique properties (i.e. good charge carrier transport properties) that make them potentially attractive for nanoscale devices such as light-emitting diodes, lasers, photodetectors, chemical/bio sensors [23]. Despite these interesting results, some aspects still limit their usability and further efforts are mainly needed to: 1) reduce the defects existing in ZnO thin films structure which, in turn, affect the sensor device lifetime and the UV emission efficiency; 2) understand the role of the native point defects (i.e. vacancies, interstitials, and antisites) controlling the electrical conductivity, property envisioned for innovative electronic applications [24].

To control the material stoichiometry it is necessary to carry out the ablation process in oxygen gas. Nevertheless, by varying the gas pressure, it changes significantly the plasma expansion regime, which in turn affects the chemical reactivity of the atomic species and, ultimately, the deposited material stoichiometry and, eventually, its morphology. In order to distinguish between gas pressure and substrate temperature, we have chosen to operate in a fixed condition, the so called shock wave regime, as established in a previous paper dealing with the properties of SnO_x thin films [25]. In this way, we were able to investigate the effect of the substrate temperature alone, without affecting the plasma expansion regime.

2. Experimental section

ZnO thin films were grown by excimer laser ablation (wavelength 248 nm, pulse width 25 ns, repetition rate 10 Hz) of a high purity (99.99%) metallic Zn target at the fixed laser fluence of 2.0 J cm^{-2} in a high purity oxygen gas atmosphere (10 Pa) for a 1 h deposition time. The substrate temperature was varied between 25 °C and 600 °C. The films were deposited onto *c*-Si and glass corning substrates positioned 45 mm from the target surface. XPS, AFM, XRD and Raman measurements were carried out on the films grown onto *c*-Si while PL characterization was performed on the corning glass deposited films. The films thickness (about 110 nm) has been measured by an Alpha-Step 500 Tencor profilometer. Further details on our PLD experimental procedures generally adopted for the growth of metal oxide thin films are elsewhere reported [25,26]. The stoichiometry of the films was determined by X-ray photoemission measurements carried out using a VG ESCALAB system. The Al Kα radiation (1486.6 eV) of a conventional twin anode Al/Mg was used as a source for the XPS measurements. Excited photoelectrons were analyzed by means of a VG Scientific CLAM 100 hemispherical analyzer operating in CAE mode with a pass energy of 50 eV. Raman spectra have been excited by the 632 nm radiation of an He–Ne laser and analyzed by a Jobin Yvon 1800 line/mm monochromator equipped with a LN_2 cooled CCD sensor. The X-ray diffraction measurements have been carried out using a Bruker D8 Advance X-ray diffractometer equipped with a Cu Kα radiation ($\lambda = 1.5406$ Å). Data were collected over a 2θ range of 30°–40°, with a step size of 0.05 at a speed of 0.05°s^{-1}. The surface morphology of the films produced was imaged by an atomic force microscope (AFM) mod. Explorer by VEECO working in contact mode. Photoluminescence spectra have been carried out using the Jobin Yvon Fluoromax-2 spectrofluorometer. The excitation wavelength, obtained from the monochromated output of a Xe lamp, was set to 330 nm. The light emitted from the sample was focused into the entrance slit of a monochromator that have a spectral grating of 1200 line/mm and it is picked up by a photomultiplier tube (PMT). A 340 nm cutoff filter was used to suppress the UV source scattered light. Plasma expansion dynamics was determined by means of fast photography imaging. Spots of the laser generated plasma were acquired using an intensified and gateable charge coupled device (Andor Technology iStar iCCD). Images of the expanding plasma were captured at different time delays with respect to the arrival of the laser pulse. A fast photodiode, used to detect a portion of the incoming laser, was used as a trigger. Integration time and intensification factor values were varied in order to maximize the signal to noise ratio.

3. Results and discussion

In Fig. 1 images of the expanding plasma at different time delays, carried out at 10 and 2 Pa of oxygen are reported. It can be clearly seen that two different expansion regimes occur at the two different oxygen pressure. In presence of 2 Pa of oxygen an isotropic expansion can be observed, the plasma shows a nearly spherical shape indicative of a free expansion regime. In presence of 10 Pa of oxygen the influence of the ambient gas becomes evident. At the interface between the plasma and the ambient gas a bright edge becomes evident pointing out for the formation of a shock wave. Light emissions from the plasma are due to relaxation processes from collisionally excited atomic species. In correspondence of the shock wave region both pressure and temperature rise, owing to collisions between plasma species and ambient gas, leading to the dissociation of molecular oxygen and to the increase of its chemical reactivity. Then, the selected deposition condition, presumably favors the formation of ZnO complexes in flight.

In Fig. 2 the wide scan XPS spectrum for the RT grown ZnO film is reported. Zinc and oxygen related peaks are evident together with very low intensity peaks due to adventitious carbon. The high resolution spectra of Zn $2p_{(3/2,1/2)}$ and O 1s core-levels are shown in the inset of the figure. The peak at 1021.8 ± 0.1 eV is due to the Zn $2p_{3/2}$, at the same energy position as in Zn bulk material [27,28]. The O 1s core-level spectrum is broadened and two peaks can be resolved by using a curve fitting procedure. The best-fit procedure was carried out by using Gauss–Lorentzian bands and a Shirley-type background function.

The component with low binding energy (530.2 ± 0.1 eV) corresponds to O^{2-} ions in wurtzite structure of hexagonal Zn^{2+} ion array. Its intensity is a measure of the amount of oxygen atoms in a fully oxidized stoichiometric surroundings [29]. The peak centered at 531.9 ± 0.1 eV is associated with O^{2-} ions in oxygen deficient regions within the matrix of ZnO. Hence this peak is a measure of the O^{2-} vacancies [30,31]. Similar trends were observed for the other samples. The O/Zn atomic ratio, *x*, was estimated by the analysis of the high resolution O 1s and Zn $2p_{3/2}$ photoemission spectra, taking into account the relative oxygen and zinc atomic Scofield's sensitivity factors [32]. It was found that all the deposited samples present a similar small oxygen deficiency (*x* ranging from 0.75 to 0.85), independently on the substrates temperature, pointing out that the growth at 10 Pa of oxygen, i.e. in the shock wave plasma expansion regime, plays the major role in determining the oxygen content of the films.

The films morphology has been investigated by AFM imaging. The results are reported in Fig. 3 where AFM images, recorded from the samples deposited at different temperatures, are shown. The surface topography changes, upon increasing the temperature, from a more fine-grained to a more coarse-grained structure as well as the roughness value ρ changes from 0.35 nm up to 5.30 nm (see Table 1). Looking at the pictures and at the roughness data, it is evident that: a relatively smooth surface characterizes the sample grown at low temperature while the films deposited at 450 °C and 600 °C show irregular and rough surfaces (see Fig. 3). Approximating the surface structure as composed by particles with a nearly circular shape, a size distribution analysis of the digital images coming from AFM has been carried out, using the SPMLab Analysis Only software. The bin-size distributions of 150 nm^2 are reported in

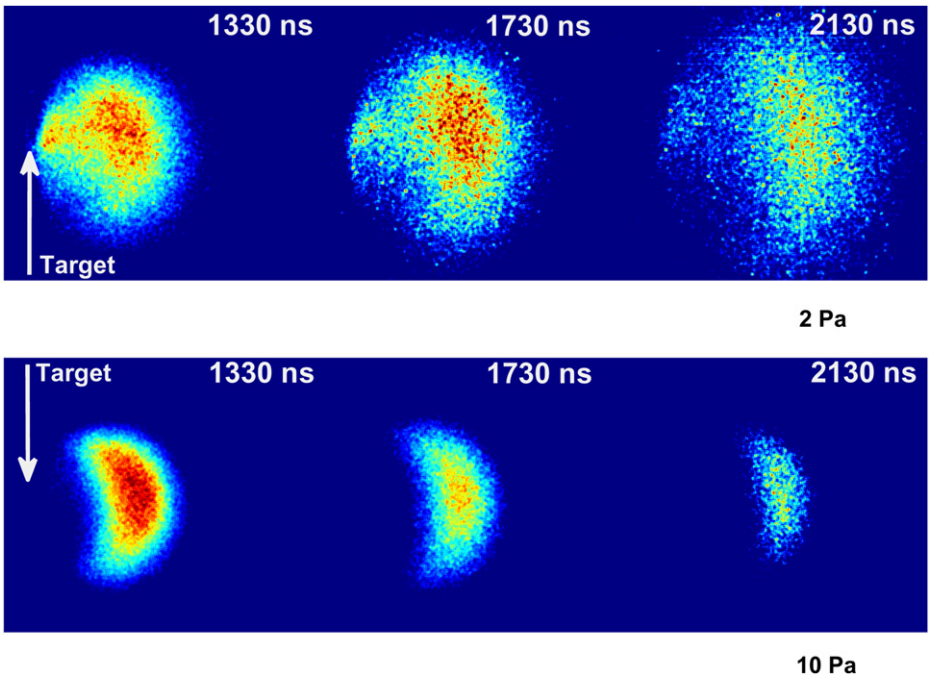

Fig. 1. CCD images of the emission of a Zn plasma at different time delays in presence of 2 and 10 Pa of oxygen.

Fig. 4. It can be clearly seen that the grains area distribution progressively broadens and shifts toward larger values upon increasing T.

X-ray diffraction (XRD) patterns of all the deposited samples, with the proper reflections assignments, are reported in Fig. 5, and well match to the standard diffraction pattern of wurtzite zinc oxide [33]. Two reflection peaks can be observed in the spectra: the first one at about $2\theta = 36.3°$, assigned to reflection from the (101) planes, while the second one at about $2\theta = 34.5°$ is originated by (002) planes reflection. In the RT deposited sample only the (101) reflection related peak is barely visible, its intensity increased in the sample deposited at $T = 150$ °C. For higher deposition temperatures its intensity is observed to decrease, and for the sample deposited at the highest temperature adopted it almost disappears. The (002) reflection peak becomes more evident at the substrates temperature of 300 °C, for samples deposited at higher temperature its intensity progressively decreases. Particularly, we observe that, at 450 °C, both the two reflection peaks are present, indicating that the film does not grow along a preferred crystallographic direction. On the overall it emerges that a kind of structural transition occurs as a function of the substrates temperature: at RT a disordered matrix is obtained and only a very small fraction of the samples show some order along the (101) crystalline direction; by increasing the substrates temperature up to 300 °C a more ordered crystalline phase appears but oriented along the (002) crystalline direction. Upon increasing further the temperature the crystalline character is progressively lost, even if some ordered phase along the (002) direction is still preserved.

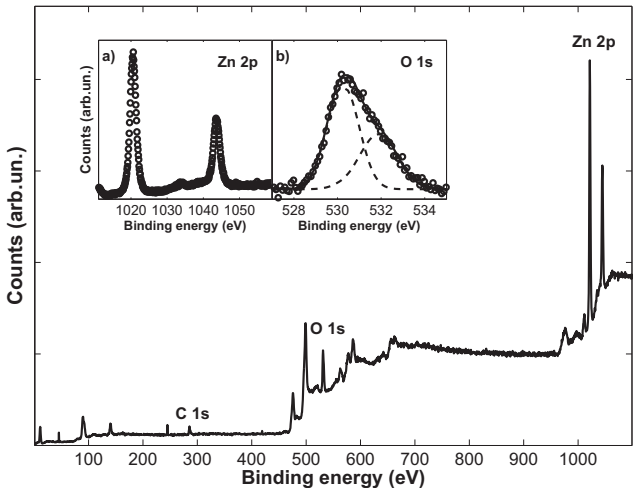

Fig. 2. X-ray photoemission spectra for the RT zinc oxide film. The results of a two subbands model fitting procedure for the O 1s photoemission peak are also reported.

The interplanar spacings d_{hkl} values were determined from the XRD features and are reported in Table 1. Keeping in mind that all films show a ZnO hexagonal (wurtzite) structure, the lattice constants a and c were calculated using the Bragg's law and from the relation: $1/d_{(hkl)} = \sqrt{4/3(h^2 + hk + k^2)/a^2 + l^2/c^2}$, where h, k, l are all integers and (hkl) is the lattice plane index [15,18]. For a perfect crystal, the ratio c/a remain almost unchanged. Deviations from this condition indicate some destroyed periodicities in the crystal planes, little-residual tensile built-in stress in the films (which probably originated by the difference in thermal expansion coefficients and lattice constants between the ZnO film and the Si substrate) and, then, a significant local distortion of the wurtzite lattice. A comparison (last column of Table 1) with the c/a ratio bulk material (2.603 Å) shows a satisfactory agreement [15], confirming that the deposited material has the ZnO wurtzite structure.

Further information, about the effect of the deposition temperature on the films structural properties, can be extracted from Raman scattering spectra. In general, the first order Raman spectrum is due to phonons near the Γ point of the Brillouin zone because of the momentum conservation rule in the light scattering process. At the Γ point, for the C_{6v} symmetry group, the hexagonal single crystal of ZnO has eight optical phonon modes: $\Gamma_{opt} = A_1 + E_1 + 2B_1 + 2E_2$ where A_1 and E_1 modes belong to polar symmetries and have different transverse (TO) and longitudinal

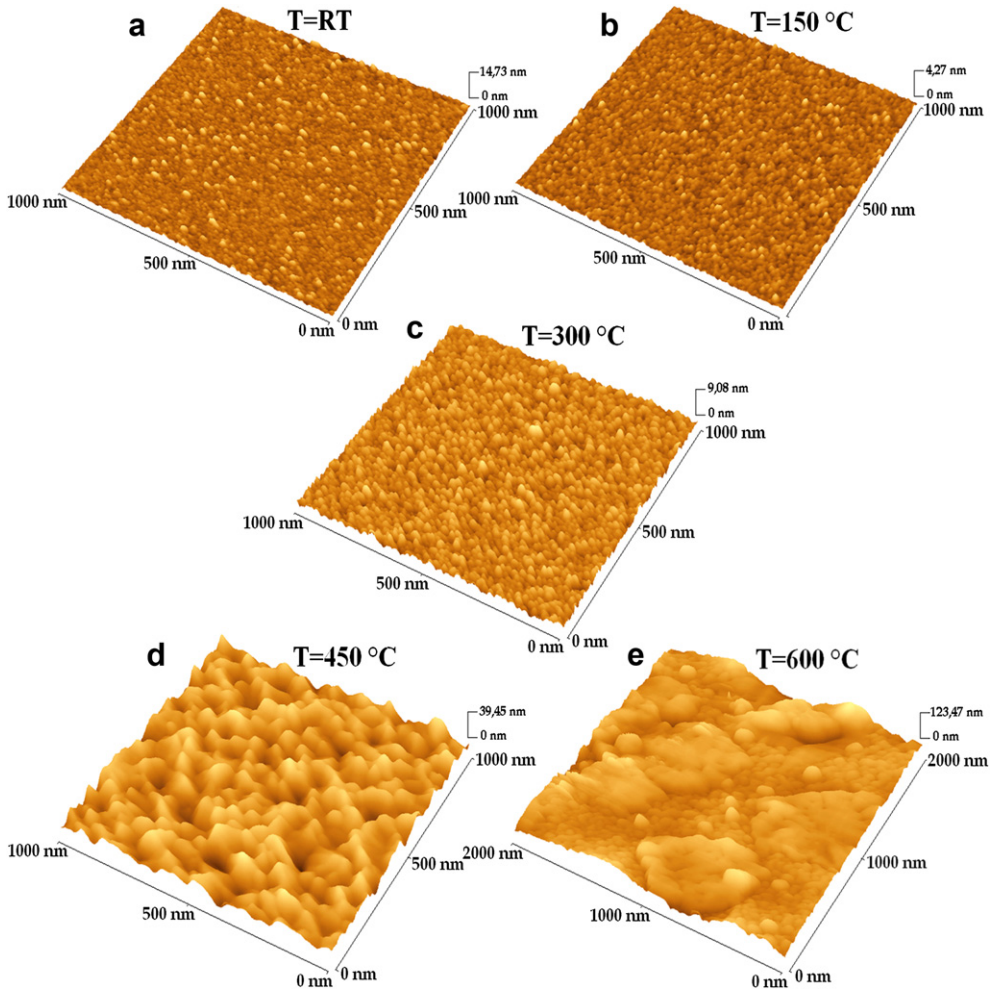

Fig. 3. AFM images of 1000 × 1000 nm^2 large areas of ZnO films deposited at RT (a), 150 °C (b) 300 °C (c), 450 °C (d) and AFM image of 2000 × 2000 nm^2 large area of the sample deposited at 600 °C (e).

(LO) optical phonon frequencies. A_1, E_1 and E_2 (low, high) modes are all Raman active, while B_1 (low, high) ones are silent [34]. Fig. 6 shows the Raman spectra of all the investigated films. The samples deposited at the lower temperatures show a very broad band in the 350–450 cm^{-1} range, due to the combination of the A_1(TO) and E_1(TO) phonon modes while the contribution around 440 cm^{-1}, attributed to the E_2-high phonon mode, is barely visible. A further broad band at about 570 cm^{-1}, assigned to the combination of the A_1(LO) and E_1(LO) modes, is well defined. This latter contribution could be attributed to the incomplete oxidation of Zn [35]. At $T = 300$ °C only the E_2-high mode, located at 440 cm^{-1}, is present. The intensity increase and the sharpness of the E_2 peak observed at $T = 300$ °C is indicative of the best crystalline quality while the downshift with respect to the frequency position of the E_2 (high) mode in ZnO standard sample (437 cm^{-1}) indicates a tensile stress in the deposited thin film. It's worth noticing that for sample grown at $T = 300$ °C this mode is the only one visible in the Raman spectrum, pointing out that the ZnO thin film grows with the c-axis oriented perpendicular to the substrate surface [36]. Upon increasing the deposition temperature up to 600 °C, all the Raman modes are still present, even if reduced in intensity and broadened.

In Fig. 7a the room temperature photoluminescence (PL) spectra obtained from all the investigated samples are shown. The PL spectra are characterized by the occurrence of different emission contributions: a main band around 3.2 eV and a broad band with some peaks superimposed in the 3.0–2.2 eV spectral range. As reported in the draft (see Fig. 7b), the band located at about 3.2 eV is the signature of the near band-edge excitonic emission, the

Table 1
Deposition conditions, film's roughness, estimated from AFM images, interplanar spacing d_{hkl} of index (hkl), obtained from the XRD patterns for different planes, the lattice constant a and c calculated from the relation: $1/d_{(hkl)} = \sqrt{4/3(h^2 + hk + k^2)/a^2 + l^2/c^2}$, where h, k, l are all integers, (hkl) is the lattice plane index and the c/a ratio.

Sample	T (°C)	ρ (nm)	$2\theta_{(002)}$ (°)	$d_{(002)}$ (Å)	c (Å)	$2\theta_{(101)}$ (°)	$d_{(101)}$ (Å)	a (Å)	c/a
ZnO1	RT	0.28	34.470	2.5997	5.1996	36.266	2.4750	3.2496	1.5995
ZnO2	150	0.35	34.465	2.6001	5.2003	36.210	2.4787	3.2558	1.5974
ZnO3	300	0.75	34.411	2.6041	5.2083	36.205	2.4790	3.2549	1.6000
ZnO4	450	4.55	34.411	2.6041	5.2083	36.211	2.4786	3.2542	1.6005
ZnO5	600	5.30	34.340	2.6093	5.2187	36.465	2.4620	3.2241	1.6135

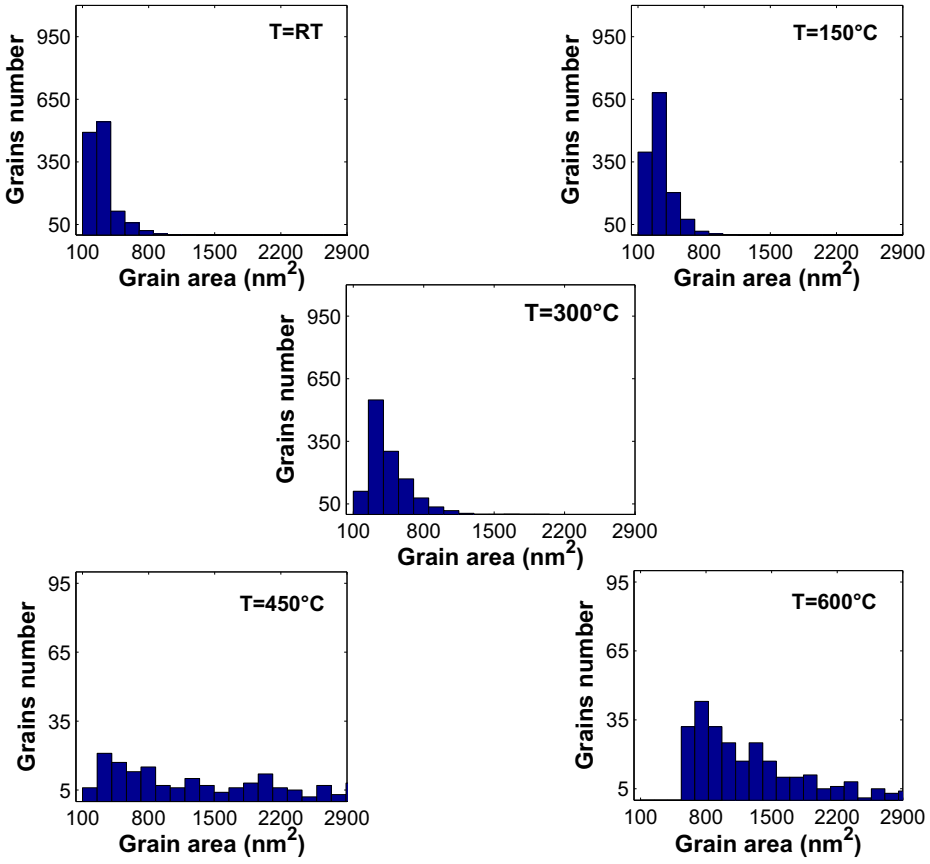

Fig. 4. Evolution of the grain number as a function of the grain area, obtained from AFM images analysis. A bin-size of 150 nm^2 was adopted.

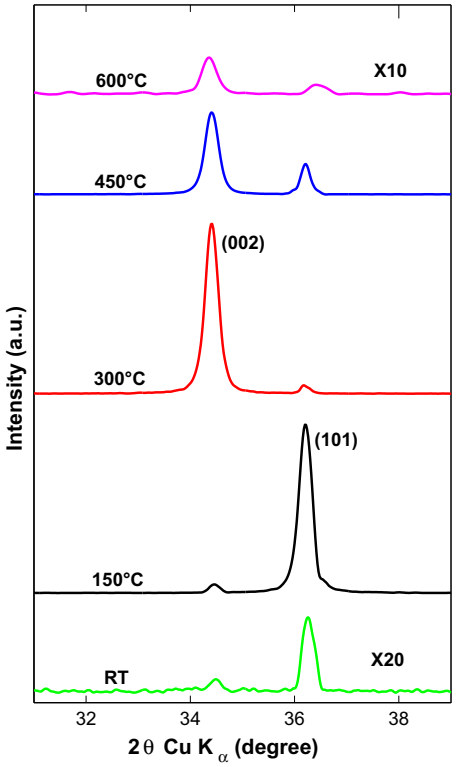

Fig. 5. XRD patterns for all the deposited samples.

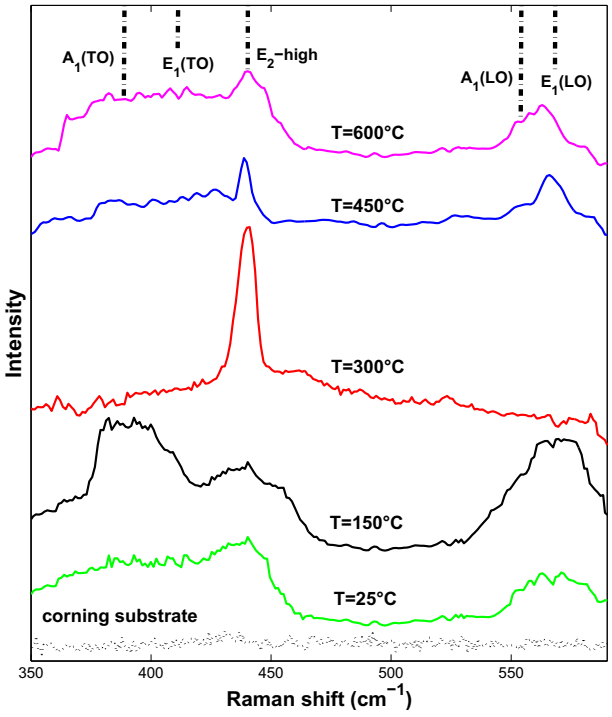

Fig. 6. Raman spectra of all the deposited samples.

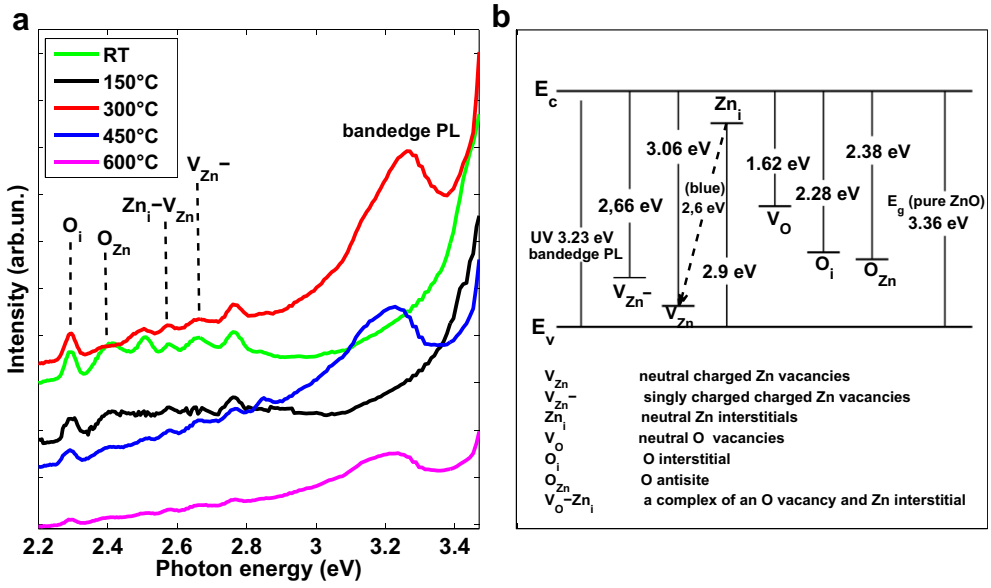

Fig. 7. (a) PL spectra of all the deposited samples; (b) draft of calculated defect-related deep level emissions for ZnO films, as reported in Refs. [35,37].

shoulder extending toward lower energies, is usually associated to the presence of neutral Zn vacancies V_{Zn} [35,37]. Some weak but well defined emission bands can be envisaged between 2.2 and 2.8 eV and are assigned to the presence of defect states, related to zinc V_{Zn} or oxygen vacancies V_O, to interstitial zinc Zn_i or oxygen O_i atoms, and antisite oxygen O_{Zn}. According to full-potential linear muffin-tin orbital calculation [35], the energy interval between the donor level of interstitials Zn and the acceptor level of Zn vacancies is about 2.6 eV, very close to the value of 2.58 eV of one of the observed emission bands.

As shown in Fig. 7a, the contribution of the UV exciton-related emission band is totally absent in the films deposited at RT and 150 °C, while the deep level emissions at lower energies are well defined. At 300 °C the band-edge appears in the PL spectrum while for the samples deposited at higher temperatures its intensity decreases.

On the overall the stoichiometry of the ZnO thin films appears to be ranged from 0.75 to 0.85 and determined by the plasma expansion regime, i.e. the shock wave one. On the other hand the substrate temperature strongly affects the structural and optical properties.

In particular, concerning the surface topography a transition from a more fine-grained to a more coarse-grained structure is observed, at the same time the roughness value ρ increases from 0.35 nm up to 5.30 nm upon increasing the temperature. This behavior points out that agglomeration of ZnO units into larger ones is favored by higher temperatures. Nevertheless best crystalline properties were observed at the deposition temperature of 300 °C, to which corresponds a film characterized by features of some tens of nanometers in size (the particles size was estimated from the areas of Fig. 4 by supposing nanoparticles with a nearly circular shape). As evidenced by XRD and Raman results, the films are preferentially (002) oriented with a surface roughness of 0.75 nm. Any further increase of the deposition temperature leads to a worsening of the film structural properties, as pointed out by the increased ρ value up to 5.30 nm and the XRD and Raman results. The intensity reduction of the (002) peak at $T = 600$ °C suggests the presence of a non-constant lattice parameter associated to intrinsic stress in presence of a large number of vacant lattice sites [22], the same considerations can be drawn from the Raman scattering spectra. As a matter of fact, it emerges that the formation of sub-stoichiometric in oxygen ZnO thin films with a preferential crystallographic orientation (as indicated by XRD and Raman data) can be tailored by controlling the substrate temperature which, in turn, determines the energy available to adatoms in order to rearrange themselves on the sample surface. In agreement with the trends shown by the above discussed results, the change of the PL response can be explained considering that when the substrate temperature is held at about 300 °C, there is an optimal balance between the substrate temperature and oxygen gas pressure, yielding a reactive velocity which leads to the formation of ZnO films with the lowest concentration of intrinsic defects [38]. On the contrary, any further temperature increase alters this balance yielding a material with higher defects concentration.

4. Conclusions

In this paper, using different spectroscopic and structural techniques, the effect of deposition temperature on the structural/morphological and optical properties of PLD deposited ZnO thin films were investigated. It was found that, operating in the shock wave plasma expansion regime, in the temperature range investigated, slightly sub-stoichiometric material were grown. The best structural and optical properties were observed when the deposition took place at $T = 300$ °C. At this temperature the ZnO thin film resulted nanocrystalline, with wurtzite crystalline structure, preferentially oriented along the (002) plane. The further increase of the deposition temperature up to 600 °C induced a worsening of the structural material's properties. As a final remark, we want to stress out the importance of carrying out the deposition process under an optimized and fixed plasma expansion regime in order not to hinder the effective influence of the substrate temperature.

References

[1] D.K. Hwang, M.S. Oh, J.H. Lim, S.J. Park, J. Phys. D Appl. Phys. 40 (2007) R387–R412.
[2] R.C. Pawar, J.S. Shaikh, S.S. Suryavanshi, P.S. Patil, Curr. Appl. Phys. 12 (2012) 778–783.
[3] K.-H. Kim, K.S. Shin, B. Kumar, K.K. Kim, S.W. Kim, J. Nanoelectron. Optoelectron. 5 (2010) 247–251.
[4] D.C. Reynolds, D.C. Look, B. Jogai, Solid State Commun. 99 (1996) 873–875.
[5] U. Ozgur, Y.I. Alivov, C. Liu, A. Teke, M.A. Reshchikov, S. Dogan, V. Avrutin, S.-J. Cho, H. Morkoc, J. Appl. Phys. 98 (2005) 041301.

[6] X. Gu, M.A. Reshchikov, A. Teke, D. Johnstone, H. Morkoc, Appl. Phys. Lett. 84 (2004) 2268–2270.
[7] C. Jagadish, S.J. Pearton, Zinc Oxide Bulk, Thin Films, and Nanostructures, Elsevier, New York, 2006.
[8] F. Oba, A. Togo, I. Tanaka, J. Paier, G. Kresse, Phys. Rev. B 77 (2008) 245202.
[9] T.R. Paudel, W.R.L. Lambrecht, Phys. Rev. B 77 (2008) 205202.
[10] H. Chen, X. Wu, L. Gong, C. Ye, F. Qu, G. Shen, Nanoscale Res. Lett. 5 (2010) 570–575.
[11] G.Z. Shen, D. Chen, C.J. Lee, J. Phys. Chem. B 110 (2006) 15689–15693.
[12] Z.L. Wang, X. Kong, Y. Ding, P. Gao, W.L. Hughes, R. Yang, Y. Zhang, Adv. Funct. Mater. 14 (2004) 943–956.
[13] Y. Zhang, G. Du, X. Wang, W. Li, X. Yang, Y. Ma, B. Zhao, H. Yang, D. Liu, S. Yang, J. Cryst. Growth 252 (2003) 180–183.
[14] S. Yoon, I. Huh, J.H. Lim, B. Yoo, Curr. Appl. Phys. 12 (2012) 784–788.
[15] T. Prasada Rao, M.C. Santhoshkumar, Appl. Surf. Sci. 255 (2009) 4579–4584.
[16] M.A. Reshchikov, J.Q. Xie, B. Hertog, A. Osinsky, J. Appl. Phys. 103 (2008) 103514.
[17] S.-R. Jian, H.G. Chen, G.J. Chen, S.C. Jason, J. Jang, Y. Juang, Curr. Appl. Phys. 12 (2012) 849–853.
[18] J. Zhao, L. Hu, Z. Wang, J. Sun, Z. Wang, Appl. Surf. Sci. 253 (2006) 841–845.
[19] J.S. Horwitz, J.A. Sprague, in: D.B. Chrisey, G.K. Hubler (Eds.), Pulsed Laser Deposition of Thin Films, Wiley, New York, 1994, p. 229.
[20] D.H.H. Hoffmann, A. Blazevic, P. Ni, O. Rosmei, M. Roth, N.A. Tair, A. Tauschwitz, S. Udrea, D. Varentsov, K. Weyrich, Y. Maron, Laser Part. Beams 23 (2005) 47–53.
[21] E. Fazio, A.M. Mezzasalma, G. Mondio, T. Serafino, F. Barreca, F. Caridi, Appl. Surf. Sci. 257 (2011) 2298–2302.
[22] B.L. Zhu, X.Z. Zhao, S. Xu, F.H. Su, G.H. Li, X.G. Wu, J. Wu, J. Liu, Jpn. J. Appl. Phys. 47 (2008) 2225–2229.
[23] Q. Wan, Q.H. Li, Y.J. Chen, T.H. Wang, X.L. He, J.P. Li, C.L. Lin, Appl. Phys. Lett. 84 (2004) 3654–3656.
[24] A. Janotti, C.G. Van de Walle, Rep. Prog. Phys. 72 (2009) 126501.
[25] S. Trusso, B. Fazio, E. Fazio, F. Neri, F. Barreca, Thin Solid Films 518 (2010) 5409–5415.
[26] F. Barreca, E. Fazio, F. Neri, E. Barletta, S. Trusso, B. Fazio, Radiat. Eff. Defects Solids 160 (10–12) (2005) 647–653.
[27] A.V. Kabashin, A. Trudeau, W. Marine, M. Meunier, Appl. Phys. A 91 (2008) 621–625.
[28] D. Guo, M. Xue, Q. Guo, K. Wu, J. Guo, E.G. Wang, Appl. Surf. Sci. 255 (2009) 9015–9019.
[29] M. Chen, X. Wang, Y.H. Yu, Z.L. Pei, X.D. Bai, C. Sun, R.F. Huang, L.S. Wen, Appl. Surf. Sci. 158 (2000) 134–140.
[30] L.M. Kukreja, P. Misra, A.K. Das, J. Sartor, H. Kalt, J. Vac. Sci. Technol. A 29 (3) (2011) 03A120.
[31] S. Venkatachalam, Y. Kanno, Curr. Appl. Phys. 9 (2009) 1232–1236.
[32] J.F. Moulder, W.F. Stickle, P.E. Sobol, K.D. Bomben, Handbook of X-ray Photoelectron Spectroscopy, Perkin-Elmer Corp., Eden Prairie, MN, USA, 1992.
[33] 20PCPDFWIN v. 2.02 ICDD (JCPDS-International Centre for Diffraction Data, 1999).
[34] K. Saravanakumar, Adv. Stud. Theor. Phys. 5 (2011) 155–170.
[35] X.Q. Wei, B.Y. Man, M. Liu, C.S. Xue, H.Z. Zhuang, C. Yang, Phys. B 388 (2007) 145–152.
[36] Y. Huang, M. Liu, Z. Li, Y. Zeng, S. Liu, Mater. Sci. Eng. B 97 (2003) 111–116.
[37] A.B. Djurišić, Y.H. Lung, Small 2 (2006) 944–961.
[38] L. Zhao, J. Lian, Y. Liu, Q. Jiang, Appl. Surf. Sci. 252 (2006) 8451–8455.